FERMILAB-PUB-14-239-PPD-TD
ACCEPTED

Thermal Design of the Mu2e Detector Solenoid

N. Dhanaraj, R. Wands, M. Buehler, S. Feher, T. Page, T. Peterson and R. Schmitt

***Abstract*— The reference design for a superconducting Detector Solenoid (DS) for the Mu2e experiment has been completed. The main functions of the DS are to provide a graded field in the region of the stopping target, which ranges from 2 T to 1 T and a uniform precision magnetic field of 1 T in a volume large enough to house a tracker downstream of the stopping target. The inner diameter of the magnet cryostat is 1.9 m and the length is 10.9 m. The gradient section of the magnet is about 4 m long and the spectrometer section with a uniform magnetic field is about 6 m long. The inner cryostat wall supports the stopping target, tracker, calorimeter and other equipment installed in the DS. This warm bore volume is under vacuum during operation. It is sealed on one end by the muon beam stop, while it is open on the other end where it interfaces with the Transport Solenoid. The operating temperature of the magnetic coil is 4.7 K and is indirectly cooled with helium flowing in a thermosiphon cooling scheme. This paper describes the thermal design of the solenoid, including the design aspects of the thermosiphon for the coil cooling, forced flow cooling of the thermal shields with 2 phase LN2 (Liquid Nitrogen) and the transient studies of the cool down of the cold mass as well.**

***Index Terms*— Cold Mass, Thermal Design, Thermal Stress Thermosiphon, Superconducting Magnets.**

I. Introduction

The Mu2e experiment consists of three magnetically coupled superconducting solenoid systems: the Production Solenoid (PS), the Transport Solenoid (TS) and the Detector Solenoid (DS). Magnetic fields generated from these magnets are used to efficiently collect and transport muons from the production target in the PS to the muon stopping target (in the DS) while minimizing the transmission of other particles. The main functions of the Detector Solenoid (DS) are to provide a graded field in the region of the stopping target and a precision magnetic field in a volume large enough to house the tracker downstream of the stopping target [1].

The Detector Solenoid coil design is based on high purity aluminum stabilized Rutherford cable. This type of conductor has been used successfully in many similar superconducting detector solenoids. The main advantage of such a conductor is that the aluminum stabilizer has very small resistivity and a large thermal conductivity at low temperatures. The DS employs two types of conductors: DS1, a "narrow" conductor in the DS gradient section and DS2, a "wide" conductor in the spectrometer section [1].

Manuscript received August 7, 2014. N. Dhanaraj (dhanaraj@fnal.gov), R. Wands, M. Buehler, S. Feher, T. Page, T. Peterson and R. Schmitt are with the Fermi National Accelerator Laboratory, Batavia, IL 60510, USA.

This work is supported by Fermi Research Alliance, LLC; under contract No. DE-AC02-07CH11359 with the U.S. Department of Energy.

The DS cold mass consists of a cylindrical 5083 aluminum shell, which houses 11 coil assemblies each comprising of DS1 or DS2 coil windings. The coil assemblies are separated by intermediate spacers that aid in achieving the necessary field distribution in the DS. The cold mass assembly is cooled by a helium thermosiphon scheme that operates at a nominal temperature of 4.7 K. The cold mass assembly is housed within a room temperature cryostat. The cold mass is shielded from the cryostat with nitrogen cooled thermal shields operating nominally at 80 K. Multi-Layer Insulation (MLI) is used to further curtail the radiation load from the cryostat to the cold mass.

This paper aims at addressing the thermal design aspects of the DS. The steady-state heat loads are addressed for both the helium and nitrogen systems. The design of the thermosiphon cooling scheme is described. The pressure and temperature conditions of the thermal shield cooling are also discussed. Finally, a transient thermal stress analysis of the DS is discussed. The results of this analysis aid in determining the temperature difference that can be safely maintained between the cold mass and the helium during the initial cool down of the magnet.

II. Heat Loads

A. Cryogenic Distribution

The cryogens for cooling the cold mass and the thermal shields will be supplied from a repurposed Tevatron "satellite" refrigerator and liquid nitrogen dewar. The cryogenic distribution begins at the refrigerator/dewar level and is transmitted to a distribution box where the flow is divided to feed the four feedboxes, which in turn serve the different solenoids of the Mu2e experiment. Figure 1 depicts the cryogenic distribution for the Mu2e experiment.

The cold mass assembly and thermal shields are indirectly/conductively cooled. The cold mass is cooled by saturated helium at 4.7 K flowing in a thermosiphon circuit and the thermal shields are cooled by pressurized two-phase nitrogen containing approximately 90% liquid at about 82 K. The helium gas returned is re-liquefied and the nitrogen gas is vented to the atmosphere.

B. Heat loads at Helium Temperatures (4.7 K)

The operating temperature of the helium bath is estimated to be around 4.7 K. The cold mass assembly will be cooled with saturated helium at 4.7 K flowing in a thermosiphon (passive heat exchange based on natural convection) circuit. The steady-state heat load contributions at 4.7 K originate from the radiation heat flux from the 80 K thermal shields and from the cold mass suspension system consisting of axial and radial supports. Table I summarizes the heat loads at helium

temperature with no contingency. Also, the dynamic heat load due to the eddy current heating has been neglected for the long charging/discharging time of the system.

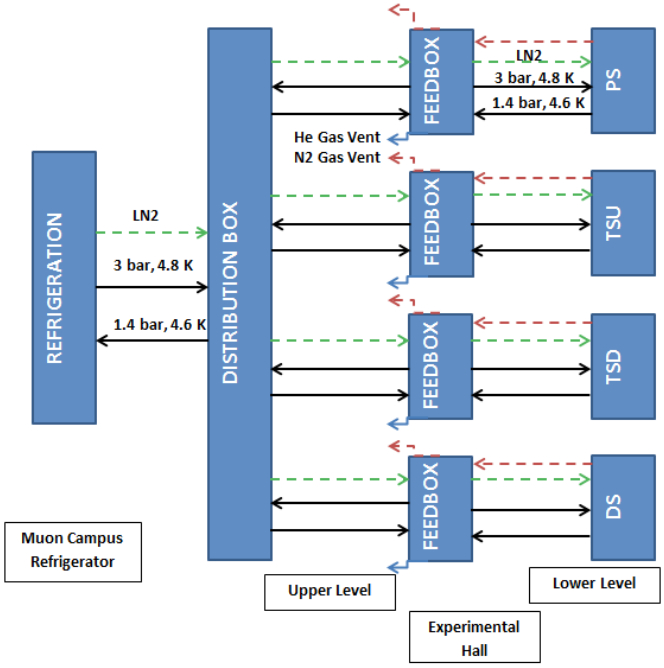

Fig 1. Schematic of the Cryogenic Distribution for Mu2e.

TABLE I
STEADY STATE HEAT LOADS AT HELIUM TEMPERATURES

Component	Heat Load in W	Estimate Basis
Radiative	30	Heat Flux at 0.2 W/m^2 [2]
Conductive (Suspension System)	2	Estimated by Integrated Thermal conductivity
Transfer Line (from Feedbox to Magnet)	4	Estimated at 0.2 W/m [3] - [5]
Feedbox	10	Engineering Estimate

TABLE II
STEADY STATE HEAT LOADS AT NITROGEN TEMPERATURES

Component	Heat Load in W	Estimate Basis
Radiative	231	Heat Flux at 1.5 W/m^2 [6]
Conductive (Suspension System)	308	Estimated by Integrated Thermal conductivity
Transfer Line (from Feedbox to Magnet)	80	Estimated at 4 W/m [3] - [5]
HTS Current Lead	60	Engineering Estimate

C. *Heat Loads at Nitrogen Temperatures (80 K)*

Two-phase nitrogen will be supplied from a Dewar at around 0.66 MPa to a phase separator in the distribution box, where it will be sub-cooled to about 90 K. The nitrogen will be then throttled to about 82 K with about 9% vapor at the inlet to the solenoids. The two-phase nitrogen will be used to cool the thermal shields, intercept the suspension system and also provide cooling for the HTS sections of the current leads. Table II summarizes the heat loads on the different components at nitrogen temperatures with no contingency.

III. COLD MASS ASSEMBLY COOLING SCHEME

A. *Thermosiphon*

The cold mass assembly will be indirectly/conductively cooled with saturated helium at 4.7 K flowing in a thermosiphon circuit. As the thermosiphon system is essentially driven by gravity, the thermosiphon tubes must be oriented vertically. The thermosiphon tubes are semi-circular segments that are skip-welded to the coil mandrel and attached at the bottom and top; to the supply and return manifolds respectively. Thermosiphon cooling concept has been successfully used to operate the ALEPH solenoids [7] and CMS detector solenoid [8]. The advantage of this system is reliability as it does not include any moving parts such as liquid helium pumps. It is also efficient as the temperature is uniform due to the fact that the cooling helium flow spontaneously adapts to the heat load distribution.

B. *Optimization of Thermosiphon Piping Components*

The sizing of the thermosiphon tubes is critical as they dictate the resulting flow quality and flow regimes. Figure 2 shows a schematic representation of the thermosiphon circuit. The thermosiphon tube sizes can be estimated by applying the energy balance principle to the set up shown in figure 3. As evidenced by the set up the total pressure gradient of the system is identically zero. Also, if the vapor quality is less than 10% the system is said to be stable [9] – [12]. Thus by applying the above information the thermosiphon tube sizes can be calculated.

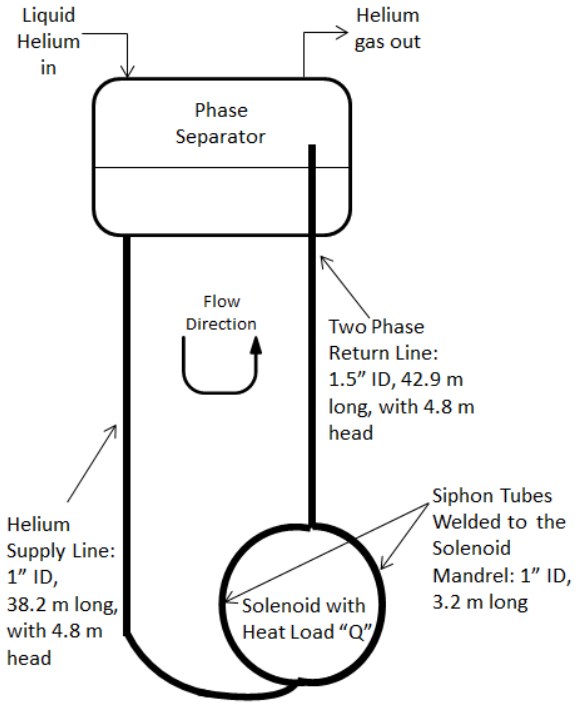

Fig 2. Schematic Representation of Thermosiphon Circuit

Furthermore, the vapor quality (~8% in our case) can be used to estimate the void fraction at the exit, which provides an indication of the flow regime [13]. As a widely accepted observation, it is best and more efficient to have the cooling scheme working in the nucleate boiling regime [10] – [12], as this provides the optimal rate of heat transfer without producing an unstable flow regime. Finally, the supply and return piping are sized to minimize the pressure drop across the thermosiphon tubes.

C. Thermosiphon Tube Location

Another major aspect associated with the design of the thermosiphon scheme is the placement of the thermosiphon tubes; especially on a large magnet such as the DS, to optimally extract the heat load from the cold mass. A sub-model (figure 3) of one of the coil modules was studied by finite element analysis approach to determine the thermosiphon tube spacing. A "distance rule" was created using this model and applied to the cold mass to extract the heat load mostly due to radiation. Although, caution was exercised to circumvent this "distance rule" near the transition between coil assemblies. Thermosiphon tubes are also planned to be installed on the spacer units which do not enclose a coil as most of the heat load in the DS is due to radiation. Thus the DS requires 49 thermosiphon tubes made of aluminum 6061-T6.

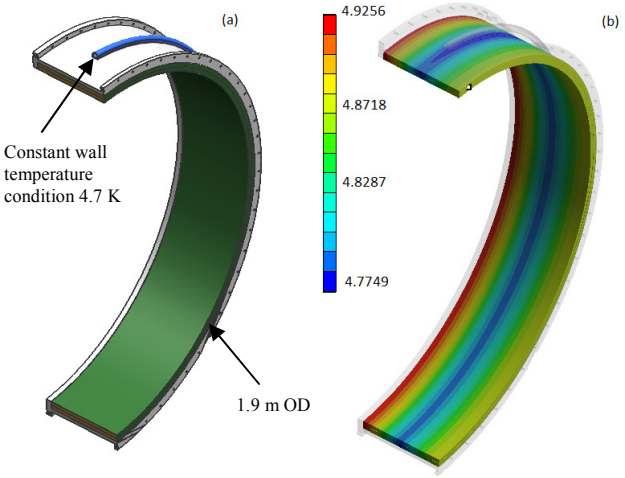

Fig 3. (a) 3D Sub-Model (b) Predicted Temperatures in the Sub-Model in kelvin.

D. Thermosiphon Tube Geometry

The thermosiphon cooling system is also designed to handle heat loads from other sources to the magnets, such as splice joints of the conductors. This interfacing aspect of the design provided advice for the thermosiphon tube geometry as shown in figure 4. The thermosiphon tubes themselves are extruded to have the fin-like features to which the cooling strips from the splices will be attached.

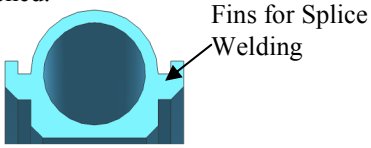

Fig 4. Thermosiphon Tube Cross Section.

E. Predicted Temperatures

The thermosiphon design was validated by means of a finite element analysis of the half symmetry model of the DS cold mass assembly. The requirements on the cryogenic distribution by the magnet design provided an operating temperature of 5.1 K for the coils. In order to accurately estimate the peak coil temperatures, the knowledge of the material properties of the cold mass assembly components including the coils became an inevitable requirement. Fourier's Law of Conduction and dedicated finite element models of the two types of conductors, DS1 and DS2, provided understanding of the conductor thermal behavior. A steady-state finite element analysis on the half symmetric model for the DS yielded estimates of peak coil temperatures. The analysis showed that the thermosiphon cooling scheme is adequately able to maintain the coil temperatures within the thermal margin as shown in figure 5.

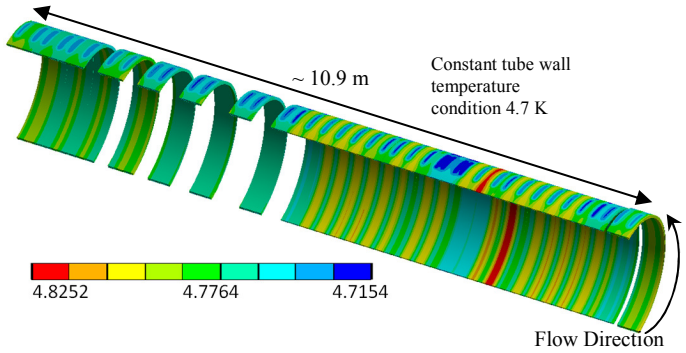

Fig 5. Predicted Temperatures in DS Coils in kelvin.

IV. Thermal Shields

The DS magnet cryostat consists of two thermal shields; inner and outer. The outer shield protects the cold mass from ambient thermal radiation and the inner shield protects the cold mass from thermal radiation, from the room temperature bore of the magnet. The thermal shields will be cooled by two phase nitrogen with about 10% vapor quality at around 0.17 MPa pressure. The advantage of this two-phase flow is that the large latent heat of nitrogen can be utilized to provide a uniform temperature cooling over a wide range of heat loads.

The inner and the outer shields are cooled in series by a 12.7 mm ID extruded aluminum 6061-T6 tube that is skip-welded to the cold mass side of the 3 mm thick thermal shields. The tube has been sized to occupy the least space while providing a low pressure drop along its entire run length and maintain a positive pressure at the end of its run as it vents to the atmosphere. An energy balance performed on the shields revealed that temperature at the warmest location on the shield (excluding some hot spots at the edges) will not exceed 85 K.

V. Thermal Stress Analysis

As part of the thermal design of the DS magnet, a thermal stress analysis has been performed to estimate the temperature difference that can be safely maintained between the cold mass and the helium supply during the initial cool down of the magnet. The cool down process can induce very high stresses

in the cold mass due to difference in thermal contraction between the different materials resulting from a non-uniform temperature distribution, i.e. the cooling tubes getting colder faster compared to the coils in the cold mass. Thus the cool down process must be controlled with optimal temperature difference that would allow for a safe cool down of the magnet. The stresses tend to be higher at the beginning of the cool down as the thermal contraction is large at warmer temperatures. A transient thermal analysis was performed to capture the highly non-linear behavior of the thermal contraction coefficient. The analysis aided in predicting the peak stresses for a specified temperature decrement from the room temperature. Indeed, 90% of the thermal contraction occurs from room temperature down to 80 K.

The DS magnet cold mass is made of different materials that are both isotropic and orthotropic. The material properties must be as accurate as possible to obtain reasonable results. Most of the material properties were obtained from well-established data sets such as Cryocomp and NIST [14], [15]. The material properties of the conductors were derived by performing finite element analysis on a stack of conductors. This stack consisted of a detailed model of all the different materials including the insulations.

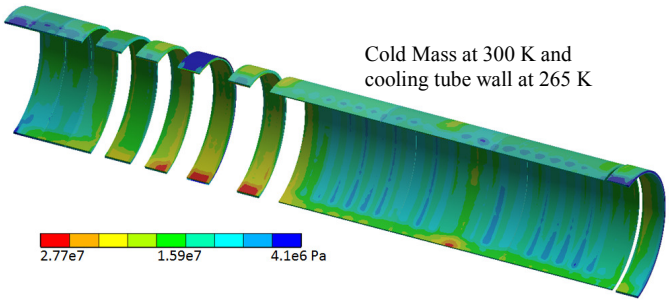

Fig 6. Von-mises Stress in the Coils after 500 seconds.

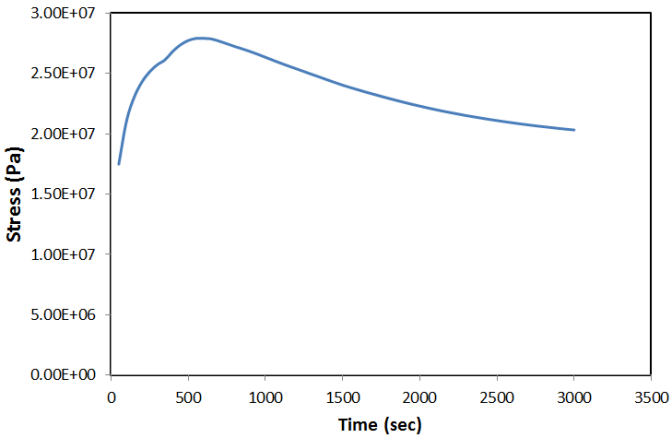

Fig 7. Maximum Stress as a Function of Time.

The thermal stress analysis was performed on a half symmetric model of the DS cold mass assembly, including the details of welds between the cooling tubes and the coil mandrel. The only thermal path for the heat transfer between the cooling tube and the mandrel was assumed to be through the welds. The coil turns were replaced by a cylindrical ring with the stack properties assigned over the entire volume. A temperature difference of 35 K was applied between the cold mass and the cooling tube inlet.

Figure 6 shows the plot of the von-mises stresses in the coils after 500 seconds into the transient run. The stresses were found to be highest at the specified time frame of 500 seconds. The maximum stress attained in the coils was about 90% of the yield of the as-received aluminum stabilizer (figure 7) for a 35 K temperature difference. The magnet requirements specify a 0.2% yield of 30 MPa for the as received aluminum stabilizer, while in reality the conductor will be cold worked to achieve improved strength.

VI. CONCLUSION

The thermal design of the DS has been described in this paper. The DS will be indirectly cooled by saturated helium at 4.7 K flowing in a thermosiphon circuit. The anticipated heat loads on the helium system from the cold mass and the heat load on the nitrogen system from the thermal shields have been discussed. As mentioned, the dynamic heat load from eddy current heating is negligible, due to the gradual charging and discharging times of the magnet. The details of the thermosiphon design have been described. Finally, a transient thermal stress analysis to estimate the temperature differences between the cold mass and the helium supply has been established.

REFERENCES

[1] S. Feher *et al*., "Detector Solenoid Reference Design Report," Mu2e Document 3664-v6, 2014, Fermilab Internal Document.
[2] D. Campi *et al*., The Magnet Project Technical Design Report, CMS TDR, 2 May 1997.
[3] G. Riddone *et al*., "Results from the Qualification of the Three Pre-Series Test Cells for the LHC Cryogenic Distribution Line," LHC Project Report 610, 15 November 2002.
[4] C. Parente *et al*., "The Local Helium Compound Transfer Lines for the Large Hadron Collider Cryogenic System," LHC Project Report 861, 1 November 2006.
[5] W. Erdt *et al*., "The Cryogenic Distribution Line for the LHC: Functional Specification and Conceptual Design," LHC Project Report 326, 1 December 1999.
[6] N. Ohuchi *et al*., "Study of Thermal radiation Shields for the ILC Cryomodule," *AIP Conf. Proc.* 1434, 929-936, 2012.
[7] J. C. Lottin and R. Duthil, "ALEPH Solenoid Cryogenic System," *Proceedings 12th Int. Cryogenic Engineering Conference*, pp. 117-121, 1988.
[8] J. C. Lottin and F. P. Juster, "Liquid Helium Thermosiphon for the 4 TESLA CMS Solenoid," *Advances in Cryogenic Engineering 43*, edited by P. Kittel, Plenum Press, 1998, pp. 1505-1511.
[9] L. Benkheira *et al*., "Heat Transfer Characteristics of Two-Phase He I (4.2 K) Thermosiphon Flow," *International Journal of Heat and Mass Transfer* 50 (2007), 3534-3544.
[10] L. Benkheira *et al*., "Heat and Mass Transfer in Nucleate Boiling Regime of He I in a Natural Circulation Loop," *AIP Conf. Proc.* 823, 871 (2006).
[11] B. Baudouy, "Heat and Mass Transfer in Two-Phase He I Thermosiphon Flow," *AIP Conference Proceeding*; 2002, Vol. 613 Issue 1, p1514.
[12] P. Bredy and B. Baudouy, *Private Communication*, July 2013.
[13] N. N. Filina and J. G. Weisend II, *Cryogenic Two-Phase Flow*, Cambridge University Press 1996.
[14] CryoComp, *Eckels Engineering* 2012, Version 5.2.
[15] http://cryogenics.nist.gov/MPropsMAY/materialproperties.htm.